17 (2023) 100304

Contents lists available at ScienceDirect

International Journal of Thermofluids

journal homepage: www.sciencedirect.com/journal/international-journal-of-thermofluids

Experimental analysis of a high temperature heat pump prototype with low global warming potential refrigerant R-1336mzz(Z) for heating production above 155 °C

Joaquín Navarro-Esbrí, Adrián Mota-Babiloni *

ISTENER Research Group, Department of Mechanical Engineering and Construction, Universitat Jaume I, Castelló de la Plana 12071, Spain

ARTICLE INFO

Keywords:
HTHP
Industrial heat pumps
Vapor compression systems
Low global warming potential (GWP)
Decarbonisation
Renewable heating

ABSTRACT

There is an urgent need to reduce fossil fuel dependency on heating processes in many sectors, highlighting industries. Vapour compression heat pumps are the most promising technologies for decarbonisation in high temperature processes. However, a climate-friendly working fluid is required for a sustainable transition. This paper presents one of the first experimental assessments of a high temperature heat pump operating refrigerant with R-1336mzz(Z). This refrigerant is an alternative to R-245fa because it is the only high temperature fluid with low global warming and zero ozone depletion potential. Fifty-one steady-state experiments were performed in a scroll compressor prototype with a liquid-to-suction heat exchanger at production temperatures between 100 and 160 °C and waste heat temperatures between 80 and 118 °C. The main considerations for the experimental campaign have been discussed, such as the control of the operational temperatures, compressor operation and liquid-to-suction heat exchanger influence. The volumetric heating capacity varied between 9.2 and 12.3 kW, and the heating coefficient of performance resulted between 1.9 and 4.4. Considering the working fluid's negligible global warming potential and high system energy performance, all considered carbon emission factors make this solution more climate-friendly than a natural gas boiler.

1. Introduction

In line with the objectives of the Paris Agreement [1], the European Union (EU) targets 2050 as the year in which the European society will be climate-neutral; this is, an economy with net-zero greenhouse gas (GHG) emissions. In 2030, climate, energy, transport, and taxation policies aim to reduce net GHG emissions to 55%, as described in the European Green Deal [2]. Cleaner energy and clean, globally competitive, and resilient technological innovation are the main benefits for the industrial sector. Given the global energy market disruption caused by the last global events, the European Commission presented the REPowerEU Plan for saving energy, producing clean energy, and diversifying energy supplies [3]. A massive scale-up of renewables, faster electrification, and replacement of fossil-based heat and fuel are listed. Thanks to the falling carbon intensity of electricity, the carbon footprint of heat pumps has been substantially reduced over the last decade. The massive use of heat pumps could provide cost-effective and practical tools for system operators to balance the variable renewable energy sources in a decarbonised power system with electrified heating [4].

Mainly focused on the human comfort application, 1.62 million heat pumps were sold in Europe in 2020 (7.4% more units than in 2019) [5]. Heat pumps can be an excellent long-term option in the European building sector compared to conventional centralised natural gas boilers systems. However, it is imperative to consider the cost of heating, which represents 27% higher than centralised boilers; in this case, gas prices tend to fall according to the high level of consumption. The cost of heating the heat pump is 18% lower than the boiler [6]. a trend towards decentralised systems and individual heat pumps can be tracked in policies, followed by research and practices. Still, the widespread deployment of this technology requires a significant enhancement in the capacity of electricity production and distribution and increasing the share of renewables in the power sector [7].

Heat pumps are Carnot limited, so starting with low-grade waste heat decreases the work required to raise to the high temperature. Typical coefficients of performance are above the unity, reducing the operating

Abbreviations: GHG, greenhouse gas; GWP, global warming potential; HTHP, high temperature heat pump; LSHX, liquid-to-suction heat exchanger; ORC, organic Rankine cycle; SHC, simultaneous heating and cooling.

* Corresponding author.
E-mail addresses: navarroj@uji.es (J. Navarro-Esbrí), mota@uji.es (A. Mota-Babiloni).

https://doi.org/10.1016/j.ijft.2023.100304
Received 31 October 2022; Received in revised form 14 January 2023; Accepted 2 February 2023
Available online 6 February 2023

Nomenclature

c_p	isobaric specific heating capacity (kJ kg^{-1} K^{-1})
COP	coefficient of performance (-)
E_{annual}	yearly electricity consumption (kWh $year^{-1}$)
h	enthalpy (kj kg^{-1})
L	yearly leakage ratio (%)
m	refrigerant charge (kg)
$\dot{m}_{ref}$	mass flow rate (kg s^{-1})
NBP	normal boiling point (°C)
P	pressure (bar(a))
PR	pressure ratio (-)
$\dot{Q}$	heat transfer (kW)
SCD	subcooling degree (K)
SHD	superheating degree (K)
T	temperature (°C)
TEWI	total equivalent warming impact (tCO_2e)
V_G	volumetric flow rate (m^3s^{-1})
VHC	volumetric heating capacity (kJ m^{-3})
$\dot{W}_{comp}$	compressor's power consumption (kW)
α	refrigerant recovered at the end of life (%)
β	electricity carbon emission factor ($kgCO_2$ kWh^{-1})

Subscripts

comp	compressor
cond	condensation
disc	discharge
evap	evaporation
in	inlet
out	outlet
xv	expansion valve

cost to become competitive and compensate for high up-front capital costs relative to boilers [8]. The levelized cost of hydrogen was nearly proportional to the coefficient of performance (COP), an energy efficiency measure. COP depends on the required temperature lift (amongst other factors, such as the compressor and refrigerant) [9]. Heat pumps are a cost-effective alternative to furnaces and air coolers. Above 30% energy efficiency can be achieved in the industries if waste heat is recovered, being particularly useful in applications like drying, pre-heating water and air, heat supply for large boilers and district heating. It is influenced by user demand, space limitations, payback period and heat pump selection methodology [10]. Moreover, heat pumps can be adapted to renewable sources such as ground source heat exchangers and photovoltaic thermal panels to increase energy efficiency [11].

The maturity of heat pumps with great temperature lift will significantly promote the application process for industrial boilers replacement [12]. At production temperatures above 100 °C (it can differ according to sources), the commonly referred to as high temperature heat pumps (HTHP) can find many uses in industry, such as chemical, paper, wood, metal, food, or textile [13]. [14] determined that 24 EU all countries are compliant with the 2050 Paris Agreement targets for heat pump integration with low-temperature lift (like ammonia production), and 21 countries are compliant with high temperature lift (like the food industry). The main constraint in 2030 is the cost, while in 2050, the main barrier is the excessive carbon intensity of electricity generation.

Electricity can be directly converted into heat or used to upgrade the steam and waste heat to make them suitable for recirculation in chemical processes, reducing fuel consumption by more than 40%. Besides decarbonisation and electrification, heat pumps can expand operating conditions by introducing more flexible processes, equipment, and energy resources [15]. Regarding district heating and cooling networks, the integration of heat pumps into small systems presents the highest potential for fossil fuel substitution, renewable energy integration, and decarbonisation. Available waste heat sources, heat requirements, and heat pump technology affect their potential [16]. As process heating in the food industry occurs below 250 °C, heat pumps could assist or completely replace the boiler to efficiently upgrade low-grade waste heat to higher temperature levels at high energy efficiency [17]. Concerning the pulp and paper industry, net-zero CO_2 emissions by 2050 (energy reduction by 23% and annual CO_2 emissions by 71%) can be achieved with fuel switching (biomass combined heating and power), improved production processes and electrification of the heat supply through the cost-optimal deployment of efficient technologies (HTHP and efficient motors). A technology deployment of heat pumps without significant policy intervention would contribute until 2050 [18]. Brough and Jouhara identified the potential of HTHP for waste heat recovery in the aluminium industry [19], particularly from reduction cell pots, compressor rooms and vertical direct chill casting or conveyors. Moreover, HTHPs could be adapted to the cement industry for revalorizing heat under conditions in which the organic Rankine cycle (ORC) is not profitable (waste heat temperature around 120 °C) [20]. The advancement in latent thermal energy storage technologies represents an opportunity for disconnecting heat recovery and heat production in HTHPs and improving the number of operating hours per year for any application, reducing the payback period [21].

The range of industries and process applicability will expand as refrigerant and compressor technologies improve and higher temperature models become commercially viable [9]. Long-term prospects for commercial application of green pure and mixture refrigerants in industrial HTHP include improving the efficiency from configuration optimisation, components improvements, safe operation, better characteristics, adaptability studies for drop-in replacements, etc. [12]. Investigations on the working fluids' heat transfer properties, durability, environmental friendliness, and effectiveness are essential to explore usage in heat pumps using molecular simulations and validating with lab-scale experiments [10]. A few experimental studies have provided publicly available data [13,22].

On the one hand, natural fluids have been explored. Wu et al. [23] built an R-718 HTHP prototype with a 30.8 m^3 min^{-1} oil-free twin screw compressor. The COP increased from 4.2 to 5.4 with 111 to 120 °C condensation temperature and a 35 °C difference. For a 45 °C temperature difference and 120 to 130 °C condensation temperature, the COP increased from 3.1 to 3.9. Bamigbetan et al. [24] tested a 48.8 m^3 hr^{-1} semi-hermetic reciprocating compressor using R-600a (initially designed for R-290). An external manifold for the discharge head and a 25% higher capacity motor were applied to expand the temperature. A liquid-to-suction heat exchanger (LSHX) allowed a maximum suction and discharge temperature of 80 °C and 140 °C. Single-stage and cascade configurations were proposed for small and large temperature lifts [25]. Average COP ranged from 2.1 for a temperature lift of 98–101 K to 3.1 for 58 to 72 K. Verdnik and Rieberer [26] investigated an R-600 HTHP based on an LSHX cycle equipped with an inverter-driven suction-gas-cooled reciprocating compressor (34.7 m^3 h^{-1} at 1450 rpm), low-pressure accumulator. A heating capacity of 30.7 kW at a COP of 4.4 was reached at a source inlet temperature of 60 °C and sink outlet from 80 to 110 °C. Trans-critical operation enables a heat sink outlet temperature of 160 °C, offering a heating capacity of 24.2 kW at a COP of 3.1.

On the other hand, synthetic refrigerants are an alternative as a trade-off solution. Mateu-Royo et al. [27] based the HTHP prototype on an R-245fa modified scroll compressor and an LSHX. At heat source temperatures between 60 and 80 °C and heat sink temperatures between

90 and 140 °C, the heating capacity and COP varied between 10.9 and 17.5 kW and between 2.2 and 3.4. Dent et al. [28] tested a new mixture (NBY-1, 132 kg $kmol^{-1}$) in a scroll compressor (14.5 kW nominal cooling capacity). 130 °C hot water was produced with a COP of 2.74 when the temperature lift was 50 °C and condensation pressure of 25.5 bar. Xu et al. [29] experimentally studied R-245fa binary mixtures. R-227ea, R-365mfc, and R-1234ze(E) are not suitable for the heat output temperature range of 80 to 100 °C, and the mixture HG-1 reached 4.9 COP at 65 and 100 °C evaporation and condensation temperatures.

HTHP for providing heat at temperatures between 100 and 160 °C have limited working fluid options. At present, only low global warming potential (GWP) R-1336mzz(Z), R-1233zd(E), R-1224yd(Z), and the mixture R-514A are available. Jiang et al. reviewed HTHPs development challenges regarding refrigerants, configuration, and components [12]. Amongst refrigerants for HTHP, R-1336mzz(Z) is the only fluid with the lowest flammability and toxicity classification (A1) in the ANSI/ASHRAE 34 standard [30].

Fan and Xi [31] demonstrated that the combination of R-245fa with R-1336mzz(Z) is the most convenient for a Carnot Battery (the former for an ORC), the latter for a heat pump) in terms of economic and exergoeconomic performance and second law efficiency. Wang et al. [32] evaluated different refrigerants for solar-driven ejector-compression hybrid refrigeration systems based on the solar radiation data in the summer of Beijing and Guangzhou. R-1336mzz(Z) did not show the highest COP but consumed the lowest electric power. [33] explored an industrial heat pump above 100 °C, considering a case study on a dairy plant. R-1336mzz(Z) can give a higher COP for the same compression ratio, evaporation temperature, and an energy cost reduction of 46%. [34] typical heat-pump-based solar district heating system with a tank store in a residential area in Germany, considering two different heat pump configurations. Systems with R-32, R-1234yf and R-1336mzz(Z) showed below-average energy efficiency.

Mateu-Royo et al. [35] compared eight advanced cycle configurations and nine refrigerants. R-1336mzz(Z) generally resulted in the highest COP increase with R-601, and R-514A, which also show the lowest volumetric heating capacity (VHC) values. Similar conclusions were obtained for configurations with ejector and economiser with parallel compression configurations [36]. For another type of configuration (based on different positions of the LSHX) [37], R-1336mzz(Z) provided intermediate values in COP and VHC, although the decrease in the second parameter is notable.

Regarding cascade configurations [38], the maximum resulting COP is 3.15 using pentane/butane, but if a low flammable solution is required to replace R-245fa/R-134a, the R-1336mzz(Z)/R-1234ze(E) is the better trade-off between safety and COP. Li et al. [39] theoretical cascade air source heat pump steam, R-134a is used in the low-temperature section of the cascade system, and R-245fa, R-1234ze(Z) and R-1336mzz(Z) are used in high temperature. The COP when R-1234ze(Z) is used is the largest, followed by R-245fa and R-1336mzz(Z). Fernández-Moreno et al. [40] concluded that R-1336mzz(Z)/R-152a/R-601 (0.8/0.16/0.05 in mass%) is the zero ozone depletion potential (ODP) and maximum safety mixture that gives higher energy performance than the rest of combinations with these constraints. The COP was 9% higher than pure R-1336mzz(Z). The potential was confirmed in a cascade model [41] to produce heat at 150 °C from a water flow at 35 °C and 25 °C.

Experimental results of R-1336mzz(Z) are abundant in ORC systems [42,43], but regarding HTHP, most previous studies are performed from a theoretical perspective [13]. Only the work of Arpagaus et al. [44] has measured the experimental energy performance of this refrigerant in an HTHP up to a supply temperature of 150 °C. Relative to R-245fa, the differences COP in the heating capacity of R-1233zd(E), R-1224yd(Z), and R-1336mzz(Z) were within the measurement uncertainty. Up to heat sink temperatures of about 110 °C, the heating capacity of R-1233zd(E), R-1224yd(Z), and R-1336mzz(Z) was 5%, 13%, and 45% lower. The integration of the LSHX resulted in a significant COP increase, and investigations of the acid number of the polyolester (POE) oils after about 100 operating hours revealed a low oil degradation. Wu et al. [23] HTHP prototype (designed for testing R-718 benefits) using R-1336mzz(Z) resulted in a COP from 4.75 to 5.75 with 86 to 125 °C condensation temperature and 35 °C temperature lift and from 2.7 to 3.3 at 45 °C temperature lift and 95 to 128 °C. Mateu-Royo et al. [27] obtained in a semi-empirical analysis that R-1336mzz(Z) has the highest COP amongst other alternatives and R-245fa measured results and higher volumetric and isentropic efficiencies at higher compression ratios. However, the VHC is around 25% lower than the other refrigerants.

Today, industrial heat pumps can only supply heat up to 180 °C, standard models with temperatures less than 100 °C, and 90 °C at heating capacity typically below 1 MW [8]. Currently, poor experimental results with climate-friendly working fluids for HTHP have been presented. More comprehensive knowledge of the behaviour of these fluids is required before they are used in machines put on the market. This paper presents the first experimental results of an HTHP equipped with a scroll compressor using R-1336mzz(Z). Another novel factor is the temperature reached by the HTHP, 160 °C, one of the highest temperatures published. The system's most significant operational and energy factors are discussed. Finally, the R-1336mzz(Z) operational carbon emissions are compared with that of a natural gas boiler, and several industrial cases have been simulated.

2. Materials and methods

2.1. R-1336mzz(Z) as HTHP working fluid

The refrigerant used in the HTHP prototype is R-1336mzz(Z). Its main properties are shown in Fig. 1 and Table 1. R-245fa's primary properties are also included for comparison as the main working fluid in HTHP.

From Fig. 1, it can be observed that R-1336mzz(Z) possesses a higher molar mass than R-245fa, but its critical pressure and heat of vaporisation are lower. Also, R-1336mzz(Z) shows a higher normal boiling point and critical temperature than R-245fa. However, R-1336mzz(Z) vapour density is remarkably lower. A higher R-1336mzz(Z) compressor size is expected in new installations and lowers heating capacity for the same compression conditions. For the same conditions, R-1336mzz(Z) would result in lower operational pressures, being in a vacuum under ambient conditions. Regarding heat exchangers design, Li and Hrnjak [45] concluded in a 24-port microchannel tube that R-1336mzz(Z) has a comparable heat transfer coefficient (HTC) and pressure gradient than other high temperature working fluid, R-1233zd(E), and a much lower HTC and higher-pressure gradient than R-1234yf and R-1234ze(E). Both refrigerants present a positive ds/dT slope. Still, Mateu-Royo et al. [46] concluded that R-1336mzz(Z) requires a minimum superheating degree between 10.1 and 19.2 K, much higher than R-245fa. If the superheating degree is provided through an LSHX, it can improve R-1336mzz(Z) COP and VHC up to 37% and 39%.

Regarding environmental characteristics, R-1336mzz(Z) is a future-proof refrigerant with a low global warming potential and zero ozone depletion potential. Concerning safety, R-1336mzz(Z) is included in the safest group, with no flame propagation and low toxicity, the latter in contrast with R-245fa. Huo et al. [47] found that reactions, environment temperatures, and the OH radical are vital in the R-1336mzz(Z) oxidation reactions. Moreover, HF, COF_2 and CO_2 are the final products in the O_2/H_2O environment, and radicals COF, O, F, CF_3, and CO_2F are also important. Huo et al. [48] showed that the dissociation temperature range of R-1336mzz(Z) with polyolester oil at 4 MPa was 250–270 °C. ReaxFF force field was carried out, and the radicals obtained from the dissociation of PEC4 ($C_{21}H_{36}O_8$) will react with R-1336mzz(Z) to dissociate it. Besides HF, CO_2 and C_2H_4 were the main decomposition products. More details about R-1336mzz(Z) regarding thermodynamic, safety, environmental characteristics and performance when used in organic Rankine cycles and HTHPs have been reviewed by Giménez-Prades et al. [49].

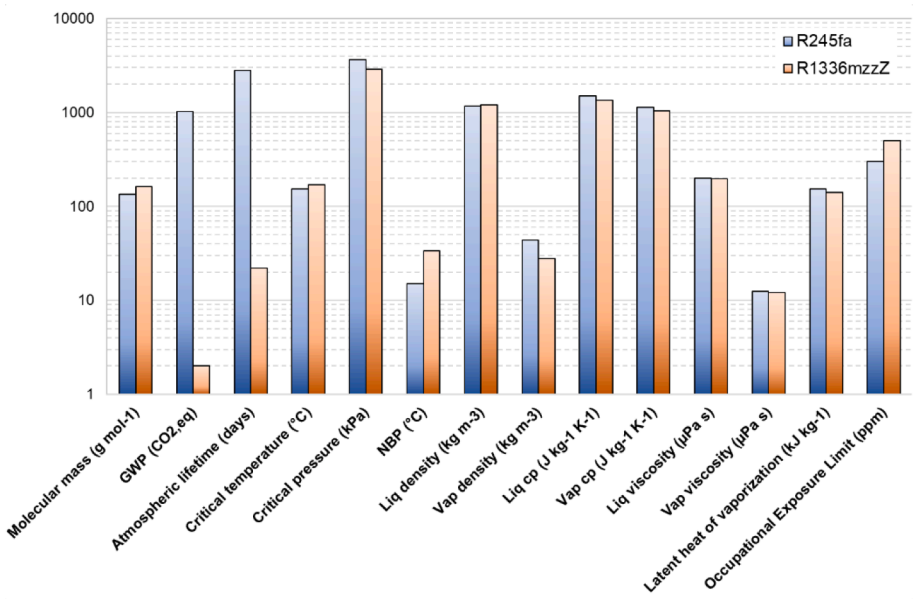

Fig. 1. Selected properties for R-1336mzz(Z) and R-245fa. Vap and Liq refer to liquid. Please refer to Table 1 for additional information not included here.

Table 1
Selected properties for R-1336mzz(Z) and R-245fa complementary to Fig. 1.

Property	R-245fa	R-1336mzz(Z)
Type of molecule	Hydrofluorocarbon	Hydrofluoroolefin
Chemical name	Pentafluoropropane	Trans-1,1,1,4,4,4-hexafluoro-2-butene
CAS number	460–73–1	692–49–9
Molecular structure	$C_3H_3F_5$	$C_4H_2F_6$
Slope ds/dT	Positive	Positive
ODP	0	0
ASHRAE safety classification	B1	A1

Table 2
Main components of the experimental HTHP prototype.

Component	Main features
Compressor	Scroll compressor, 7.5 kW and 22 m^3 h^{-1} at 50 Hz
Condenser	Brazed plate type, 86 plates, heat exchange area of 5.3 m^2
Evaporator	Brazed plate type, 48 plates, heat exchange area of 6.1 m^2
LSHX	Brazed plate type, 50 plates, heat exchange area of 3.0 m^2
Expansion valve	Electronic expansion valve

2.2. Experimental setup

This section exposes the experimental setup designed and built to operate as the HTHP. The configuration selected is an LSHX vapor compression cycle with a set of secondary circuits to simulate the heat sink and heat source. A picture of the system and a schematic diagram are shown in Fig. 2. The details about the main components of the vapour compression circuit are listed in Table 2.

Besides the main components mentioned in Table 2, other secondary components are present in the circuit, such as a liquid receiver, filter dryer, bypass valves, auxiliary expansion device, etc. Pipelines, heat exchangers and other components are insulated to avoid thermal losses to the ambient and dissipate heat to the heat sink.

Three secondary circuits set the evaporation and condensation conditions based on thermal oil as heat transfer fluid. The heat sink is then cooled in a water-cooling circuit, including a rooftop dry cooler whose frequency is controlled by a proportional-integrative-derivative (PID) controller. A 13 kW electric boiler controls the load required in the heat source through a PID controller. All three circuits have auxiliary components for safe operation at high temperatures and frequency-controlled circulating pumps.

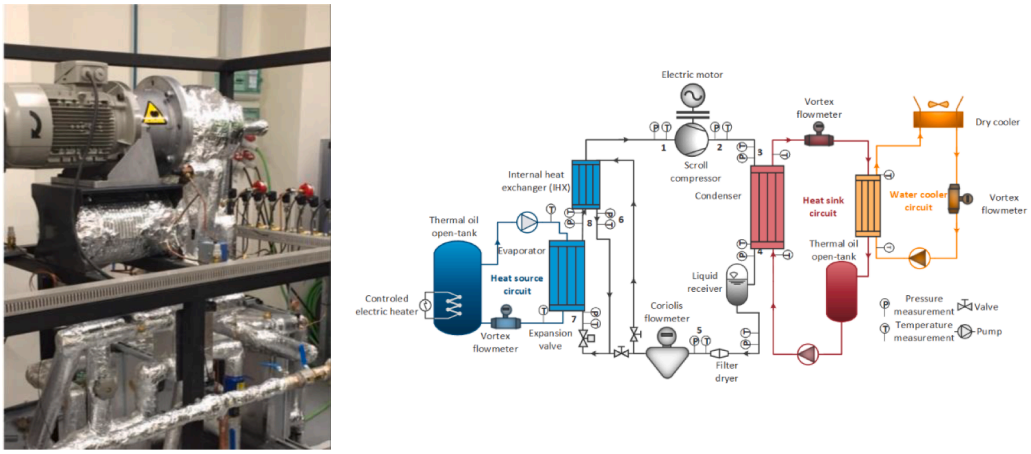

Fig. 2. Picture and schematic diagram of the experimental HTHP prototype.

All necessary information to characterise and validate the vapour compression operation and energy and thermal efficiency is retrieved from calibrated sensors. Therefore, temperature and pressures at the inlet and the outlet of each component, the mass flow rate in the liquid line and compressor power consumption are measured in the primary circuit, and temperatures at the inlet and the outlet of the circuit and volumetric flow rate in the secondary circuits. The thermodynamic states of R-1336mzz(Z) are determined using REFPROP v10.0 [50]. The summary of sensors technology and uncertainties is included in Table 3.

2.3. Experimental measurements

The targeted steady-state points are recorded for 5 min with a sampling period of 1 second when all critical circuit temperatures are identified as stable. The maximum deviation for the heat sink and source temperatures was ±0.3 K and ±0.15 K. The acquired raw measurement data is saved in columns in a text file and then further processed through a computer program developed in a MATLAB environment. Steady-state operational data points are determined by averaging the raw measurement data over a filtered file.

The test campaign covered a wide range of temperatures, as shown in Table 4. The aim is to provide a wide range of points for calculating the experimental COP and developing the semi-empirical model. The highest outlet sink temperature (heat sink outlet) was below 160 °C because of technical limitations. The heat source temperature varied from 82 °C at the inlet and starting from 69 °C at the outlet of the evaporator. At some point, the frequency of the inverter was reduced from 50 to 40 Hz, not to be limited by the electric boiler connected to the heat source secondary circuit.

The uncertainty propagation methodology for all the calculated parameters are described in Mateu-Royo et al. [27]. The uncertainty propagation was calculated using a function implemented in Engineering Equation Solver software and shown in error bars in the figures included in the results section.

2.4. Equations

This subsection presents the equations required to determine all the operational and energy parameters discussed in the paper.

The compression pressure ratio, Eq. (1) is the ratio between the discharge and suction pressure measured at the corresponding lines.

$$PR = \frac{P_{disc}}{P_{suc}} \tag{1}$$

Total superheating and subcooling degrees Eq. (2) and ((3), respectively) are obtained using pressure measurements to determine the condensation and evaporation pressures and temperature measurements at the inlet of the compressor and expansion device. Therefore, these parameters include LSHX liquid subcooling and vapour superheating.

$$SHD = T_{suc} - T_{evap} \tag{2}$$

Table 3
Overview of sensors uncertainties.

Measured parameters	Sensor	Uncertainty
Temperature	J-type thermocouples	±0.3 K
Pressure	Piezoelectric pressure transducers	±0.04% of reading
Refrigerant mass flow rate	Coriolis mass flowmeter	±0.17% of reading
Heat source volumetric flow rate	Vortex flowmeter	±0.5% of reading
Heat sink volumetric flow rate	Vortex flowmeter	±0.028 $m^3\ h^{-1}$
Compressor power consumption	Digital wattmeter	±1.55% of reading

Table 4
Range of main operational conditions in experimental tests.

Parameter	Range
Heat source inlet temperature (°C)	83–117
Heat source outlet temperature (°C)	69–86
Heat sink inlet temperature (°C)	89–136
Heat sink outlet temperature (°C)	102–158
Total superheating degree (K)	17.6–32.4
Total subcooling degree (K)	17.6–32.2
Compressor frequency (Hz)	40 and 50

$$SCD = T_{xv,in} - T_{cond} \tag{3}$$

The specific heating capacity is the enthalpy difference between the inlet and the outlet of the condenser. Then, this parameter is used for calculating the heating capacity when multiplied by the refrigerant mass flow rate, Eq. (4).

$$\dot{Q}_{cond} = \dot{m}_{ref}(h_{in} - h_{out})_{cond} \tag{4}$$

The heating coefficient of performance (COP) refers to the heating capacity divided by the compressor power consumption, Eq. (5). The simultaneous heating and cooling COP (SHC COP) considers the heating and cooling capacities as the output of the system. In contrast, the compressor power consumption remains the input (Eq. (6)). The cooling capacity is determined by multiplying the specific enthalpy difference at the evaporator by the refrigerant mass flow rate.

$$COP = \frac{\dot{Q}_{cond}}{\dot{P}_{comp}} \tag{5}$$

$$SHC\ COP = \frac{\dot{Q}_{cond} + \dot{Q}_{evap}}{\dot{P}_{comp}} \tag{6}$$

The Total Equivalent Warming Impact (TEWI) metric is obtained as shown in Eq. (7), composed of the direct accidental refrigerant leakage during operation and recovery and the indirect carbon emissions due to electricity consumption.

$$TEWI = m\ GWP\ L\ n + m\ GWP\ (1-\alpha) + E_{annual}\ \beta\ n \tag{7}$$

The rest of the parameters are directly measured in the experimental setup or obtained using REFPROP v10.0 [50].

3. Results and discussion

3.1. Operational results

This section shows the experimental measurements and calculations of the main parameters related to the regular operation of an HTHP based on a vapour compression cycle. This will help identify the unit's suitability as a renewable heating production technology in the temperature range of 100 to 155 °C, which fossil fuel burners still dominate today.

Evaporation temperatures ranged from 66 to 85 °C and condensation temperatures between 101 and 153 °C. Evaporation and condensation temperatures are determined by averaging the pressure sensor measurements at each component's inlet and outlet and then considering the two-phase or saturated state. As a pure refrigerant, the phase change (evaporation/condensation) occurs at a constant temperature, only variating due to the slight pressure loss in the components. These components (plate heat exchangers) have been designed and selected to minimise pressure losses. The experimental setup required higher evaporation temperatures to reach higher condensation temperatures, limiting the compressor pressure ratio and discharge temperature values, as shown in the following.

The compressor pressure ratio is the following parameter studied in this section, directly obtained by the pressure transducers installed in

the compressor discharge and suction lines. The pressure ratio is one of the most influential parameters in the compressor's operational and energy efficiency. As shown in Fig. 3, the experimental setup reached higher pressure ratios at higher evaporation temperatures, meaning a higher temperature difference between the heat source and heat sink. As discussed before, the evaporation level followed the increase of the condensation level but to a lower extent in most conditions. It was mainly limited to the most critical conditions, high condensation temperature, because an excessive discharge temperature must be prevented. Frequency change has an almost negligible effect on the compressor pressure ratio, considering that a decrease in the compressor frequency reduces refrigerant velocity; hence, refrigerant pressure drop at the suction and discharge lines and ports are lowered.

This observation results in a constraint for the HTHP prototypes addressed to the industrial sector. If higher heating production temperatures were reached with this proposal, the unit would require a higher heat sink temperature to ensure an appropriate lifetime. In the absence of heat sinks of suitable temperature, the configuration must be changed from a one-stage to a multi-stage compression or cascade.

The total superheating and subcooling degrees, amongst other operational parameters, are in Fig. 4. The total superheating degree is influenced by the evaporator superheating, controlled by the electronic expansion valve, and the LSHX additional superheating. In contrast, the final value measured is lightly reduced by the thermal losses in the suction pipeline and other accessories. On the other hand, the total subcooling degree comes from the subcooling in the condenser, liquid pipeline and LSHX (all elements contribute to an increase in the final value).

It is observed as both parameters follow a similar trend, increasing at higher pressure ratios. Considering that the evaporator and condenser superheating and subcooling degrees are almost constant, the pressure ratio influences the LSHX thermal effectiveness, increasing the final superheating and subcooling degrees. As most of the pipelines and accessories in the suction and liquid lines are thermally insulated, the effect mentioned above is the only one that dominates the observed variation. A minimum total (or suction) superheating degree is essential in R-1336mzz(Z) to have a dry compression, and values above 20 K are usually recommended in the literature [46]. The literature also proved the benefit of LSHX in HTHPs, so this component primarily provides the total superheating degree.

Most theoretical works comparing the effect of the LSHX have observed beneficial effects on the energy efficiency of the HTHP. For a heat exchanger operating at varying conditions, the thermal effectiveness varies, increasing higher temperature difference. Keeping the condenser and evaporator subcooling and superheating degrees constant, the inlet of the temperatures at the entrance is kept constant. Fig. 5 shows the LSHX heat exchange effectiveness, which is strongly dependant on the pressure ratio (and hence, the temperature difference between inlet temperatures). At a higher-pressure ratio, the difference between the evaporator outlet (LSHX cold side inlet) and condenser outlet (LSHX hot side inlet) temperatures grows, as does the LSHX thermal effectiveness. Besides temperature difference, LSHX is also influenced by the construction, configuration (countercurrent flow) and design. In HTHP technology, it is essential to size LSHX considering critical conditions (for operating at the highest pressure ratio and condensation temperature) to limit the maximum achievable discharge temperature.

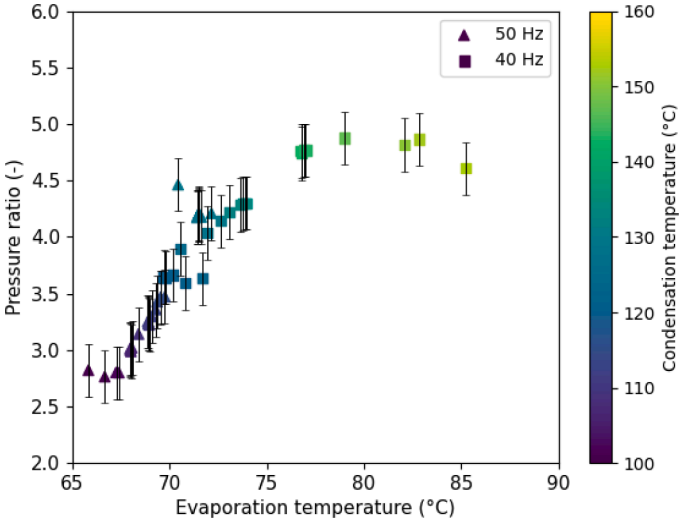

Fig. 3. Pressure ratio at different evaporation temperatures.

Besides vapour quality at the inlet of the evaporator (assuming isenthalpic expansion) and hence refrigerating effect, LSHX also affect suction density. In pure refrigerants, suction density depends on the total superheating degree, pressure losses in the low-pressure side of the circuit (evaporator and suction sections), and the working fluid. Fig. 6 shows the evolution of suction density for all experimental measurements, determined using REFPROP v10.0 [50]. It can be seen as it increases affected by evaporation temperature, and the change of compressor frequency has a minimum beneficial effect on it since a decrease in the compressor rotational speed reduces refrigerant mass flow rate and velocity, and pressure losses.

The refrigerant mass flow rate depends on compressor characteristics and operation, which is considered constant besides the frequency change in the 70–75 °C evaporation range, suction density, and volumetric efficiency. As it is observed in Fig. 6, the measured mass flow rate grows with suction density. Compared with R-245fa's previous experimental results [27], the mass flow rate can be considered low. This effect is not a problem since a lower heating capacity can compensate for a higher frequency operation or compressor.

Fig. 7 represents the measured production temperature, meaning the temperature at which the secondary circuit thermal oil is heated (applicable process temperature in industrial applications). This parameter is essential because HTHP's successful deployment is limited by the maximum temperature of the current flow delivered. As can be seen, this parameter varies between a minimum of 102 °C at 68 °C evaporation temperature and 100 °C condensation temperature and 158 °C at 87 °C evaporation temperature and 155 °C condensation temperature. At 70 °C evaporation temperature, heat is delivered at 130 °C at a similar value of condensation temperature. The condenser and HTHP design make the condensation temperature a limiting factor for reaching higher temperatures. A proper heat exchanger condenser design reduces the pinch point, approaching the production temperature to the condensation temperature. Attending to the measurement at the condenser inlet, most desuperheating was dissipated in the discharge section (port, line, connections, etc.). Therefore, the temperature entered the condenser close to the vapour saturation point. The change in compressor frequency does not influence the production temperature; HTHP heating capacity could be modulated through this parameter without affecting a critical parameter such as the production temperature. As seen in the literature [12], 158 °C is one of the highest production temperature values published today.

The heating effect is presented in Fig. 8. This parameter represents the enthalpy difference registered at the condenser (determined using temperature and pressure measurements). Therefore, it contributes to calculating the total heat delivered and the mass flow rate. Conditions with higher evaporation temperatures could result in a higher heating effect in heat pumps because of a more significant desuperheating contribution. However, the latent heat of condensation decreases at higher condensation temperatures, representing most of the heat that can be provided to the heat sink. Moreover, in this HTHP experimental setup, and due to the high temperature at the compressor's discharge, most of the sensible heat is transferred to the ambient in the discharge section, taking place most of the desuperheating process outside the

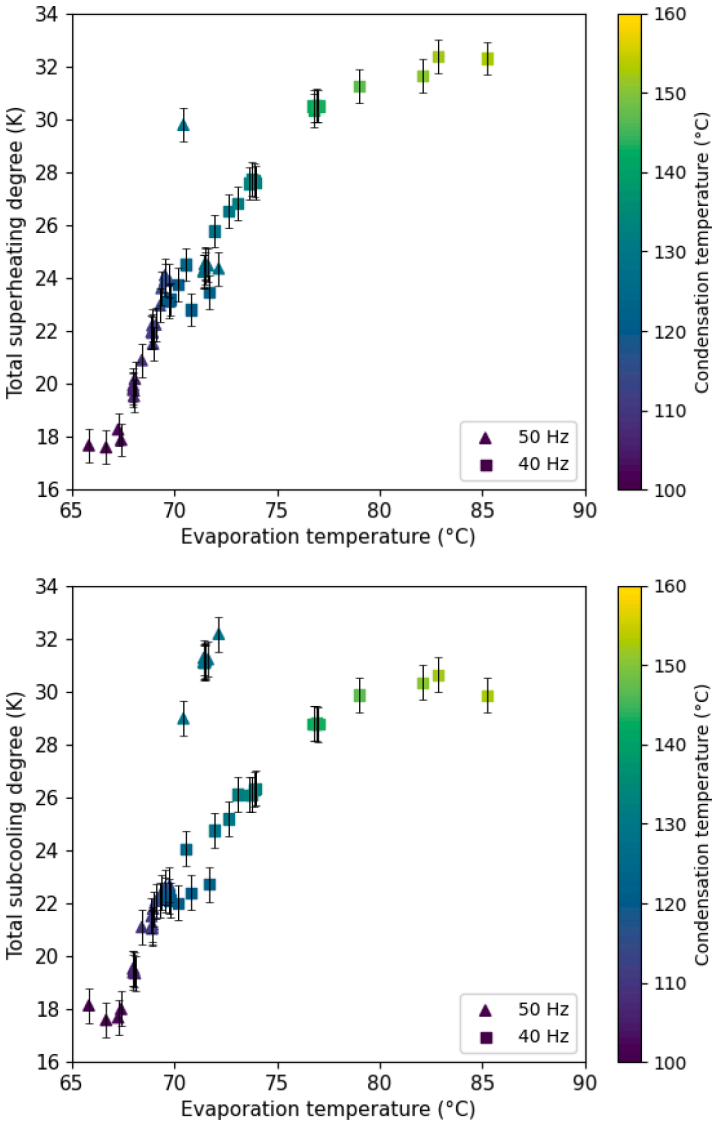

Fig. 4. Total superheating and subcooling degrees at different evaporation temperatures.

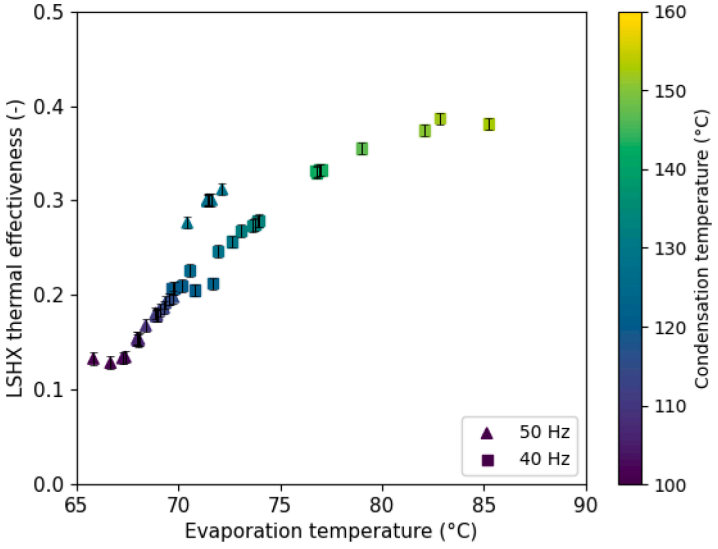

Fig. 5. LSHX thermal effectiveness at different evaporation temperatures.

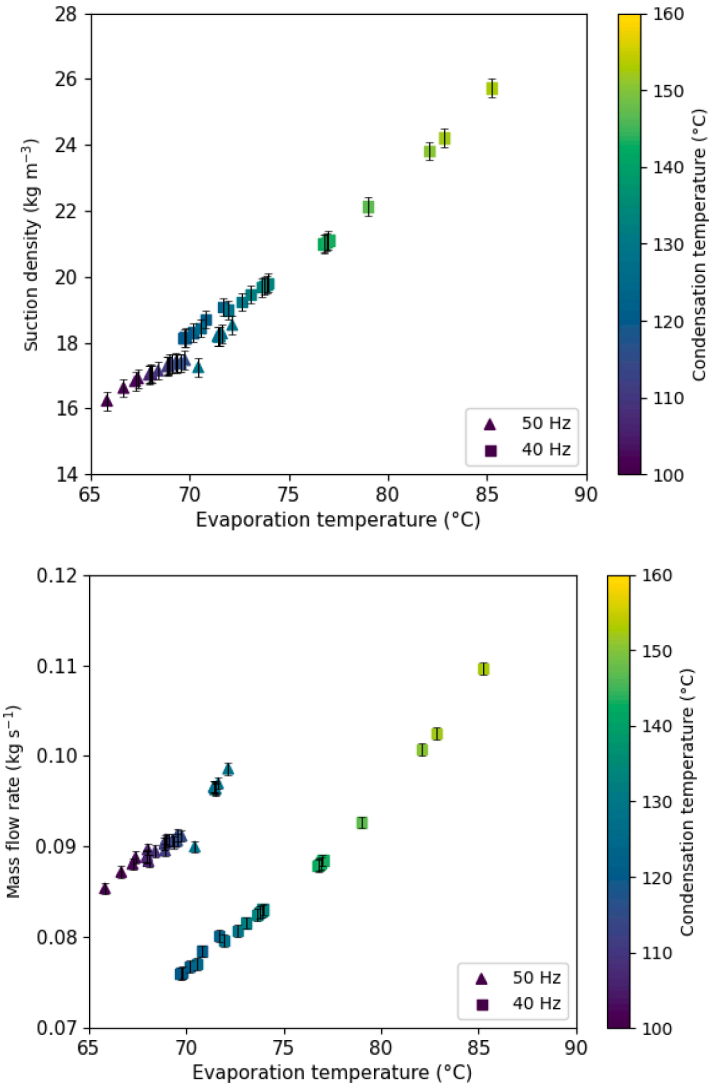

Fig. 6. Suction density and mass flow rate at different evaporation temperatures.

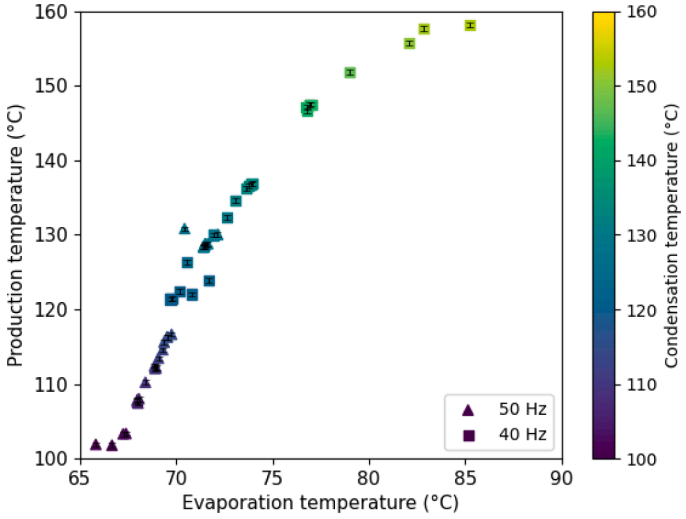

Fig. 7. Production temperature at different evaporation temperatures.

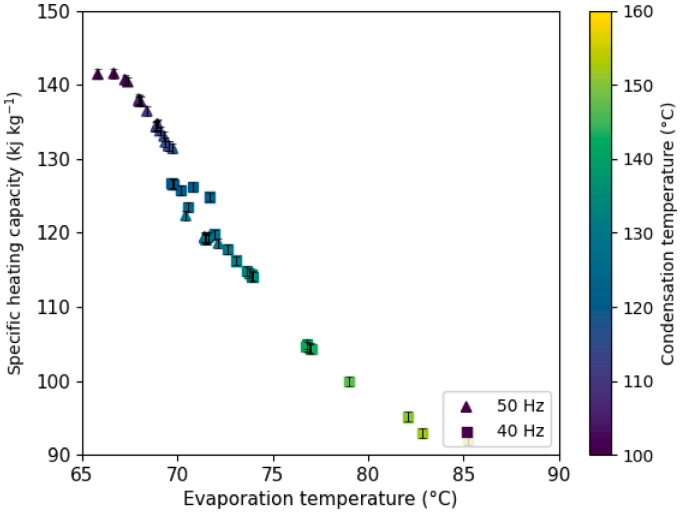

Fig. 8. Heating effect at different evaporation temperatures.

condenser.

3.2. Energy results

Fig. 9 includes the condenser heating capacity, determined as the product of the mass flow rate measured by the Coriolis mass flow meter in the liquid line and multiplied by the heating effect. Affected by the evaporation and condensation temperatures, there is an opposite contribution of mass flow rate and heating effect to the variation of this parameter. While mass flow rate increases heating capacity at higher operational temperatures, heating capacity reduces it. Therefore, the resulting variation depends on the contribution of each parameter. All in all, variation for the same compressor frequency is not remarkable, so the nominal heating capacity is kept for the different operational conditions tested (approximately 12 kW at 50 Hz and 9.5 kW at 40 Hz).

Compressor power consumption is directly measured from the compressor frequency inverter; therefore, it considers all irreversibility of the compressor (overall compressor efficiency, including electromechanical, isentropic and volumetric). As depicted in Fig. 10, the compressor power consumption grows at higher evaporation pressure due to the mass flow rate (influenced by suction density and frequency) and the higher total superheating degree at the compressor suction, as analysed before. Moreover, the compressor frequency's adaptation at the 70–75 °C evaporation temperature range reduced the rise of power consumption. For the same evaporation temperature, it is seen that the condensation temperature has an influence, but in this case, minor since it only influences the pressure ratio and efficiencies. Values measured vary between 2.75 at 65 °C evaporation and 100 °C condensation temperature and 5.3 at 87 °C evaporation and 155 °C condensation temperature.

The coefficient of performance represents the energy efficiency of the heating production system based on a vapour compression cycle. The maximum value is determined by the reverse Carnot efficiency and is limited by the operating temperatures of the circuit. Given the many irreversibilities existing in this experimental setup, the COP is far from the expected ideal values. However, as it is above the unity and the refrigerant has a low GWP, this heating production system based on electricity will always result in a lower operational carbon footprint than a set of resistances.

The maximum COP reached in the system, 4.5, occurs at 67 °C evaporation and 100 °C condensation temperatures, as shown in Fig. 11. If the requirement of the industrial plant allows these conditions, the energy and environmental benefit would be remarkable. When the condensation temperature increases, the evaporation temperature

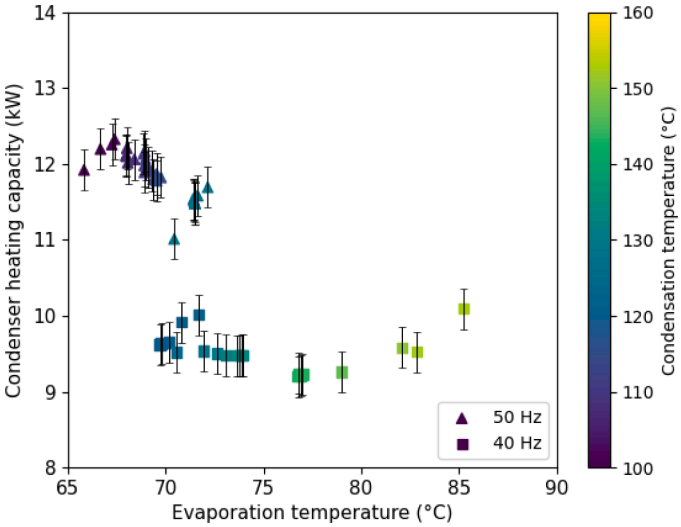

Fig. 9. Condenser heating capacity at different evaporation temperatures.

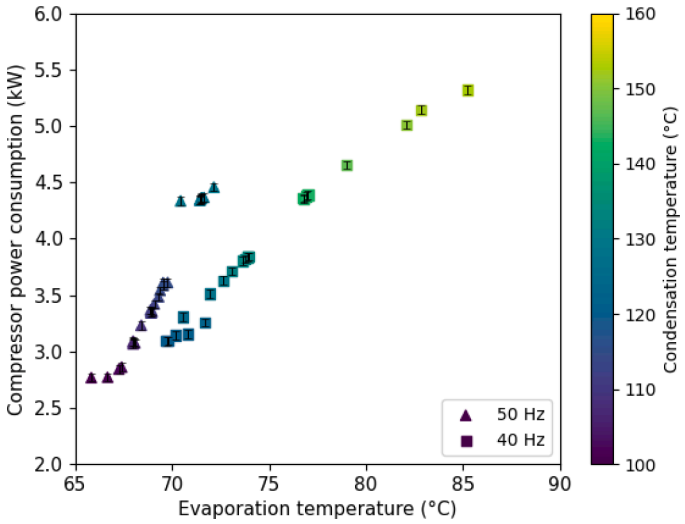

Fig. 10. Compressor power consumption at different evaporation temperatures.

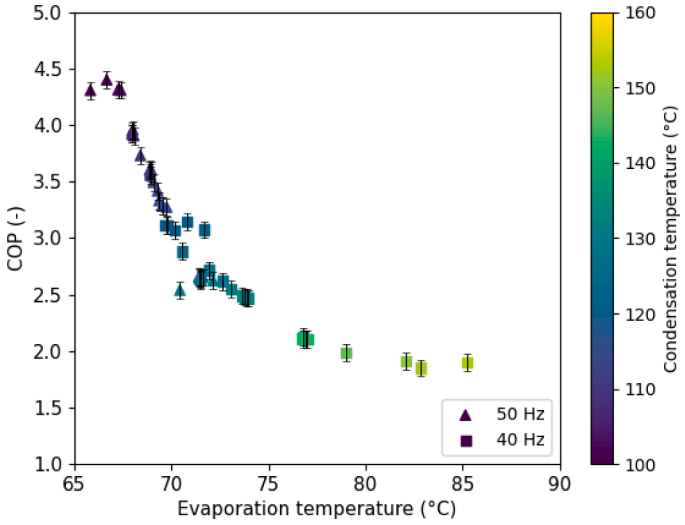

Fig. 11. COP at different evaporation temperatures.

increases but to a lower extent, so the pressure ratio increases, and the COP is reduced. For instance, the COP is approx. 3 at 70 °C evaporation and 120 °C condensation temperatures, and from 70 °C, it remains around 2.0 even in the maximum production temperature of the system, 155 °C condensation and 85 °C evaporation temperatures. The COP is slightly affected by the change in compressor frequency (if compared with pressure ratio), as it influences the compressor losses and pressure drop in the circuit. Analysing the values of COP reached by the system, it can be concluded that it is a convenient solution for renewable heating production in all the tested temperature ranges.

COP parameter refers to the heat pump's energy efficiency if the only product is heating. However, vapour compression systems can be connected to (a minimum of) two processes. Besides heating, cooling is possible in another industrial process with the same electrical input (typically provided by an individual chiller). Therefore, given the current situation regarding gas and electricity prices and availability, it is imperative to this condition of the HTHP. Therefore, for determining the simultaneous heating and cooling (SHC) COP, the heating and cooling capacity of the HTHP is considered the output (the same compressor power consumption input).

This parameter is presented in Fig. 12. Considering both thermal

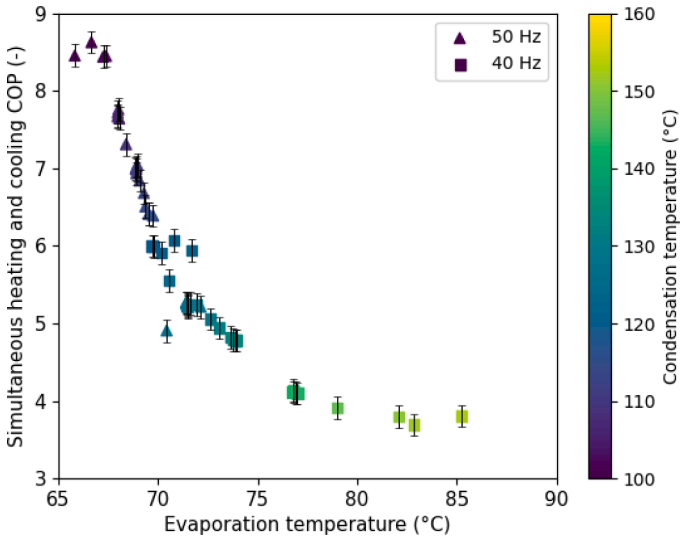

Fig. 12. SHC COP at different evaporation temperatures.

exchanges, the COP can reach up to 8.5 values at low evaporation and condensation. As the heating COP, cooling COP (or Energy Efficiency Ratio) also decreases with the pressure ratio. Therefore, the decrease of SHC COP at higher condensation conditions is more aggravated. However, in the most adverse conditions for energy efficiency, the SHC COP is above 3.5. The energy benefit of using HTHP in SHC applications is highlighted in these experiments. However, there are still challenges associated with combining industrial applications, energy dissipation, or thermal energy storage.

3.3. Carbon footprint

In this section, the carbon footprint assessment is based on the above-discussed experimental results regarding heating COP. Five operational conditions have been selected to represent different temperature levels that can be found in the industry. Moreover, four carbon emission scenarios are established, simulating a negligible (Sweden), low (Brazil), medium (United States) and high (China) electricity carbon emission factor. The refrigerant charge has been from the directly used in the installation and is kept constant. Despite the almost negligible GWP value of R-1336mzz(Z), remember that this HTHP is a prototype; therefore, equipment with much lower charge requirements can be designed. The rest of the parameters are commonly proposed in TEWI guidelines. The main assumptions of the TEWI analysis are summarised in Table 5.

The results selected for the TEWI analysis are included in Fig. 13. In the country with the lowest GHG electricity carbon emission factor, and hence, indirect TEWI contribution to the total emissions, direct emissions represented 1% of the total. Moreover, a natural gas boiler (2.15 $kgCO_2e$ per Nm^3) would emit in the same period and for the same heating capacity, 242.3 tCO_2e. This value is not reached by any country, being the HTHP conditions in the worst condition (80 °C evaporation temperature and 150 °C condensation temperature and carbon emission factor of China), 32% lower than the natural gas boiler. Therefore, the convenience of the HTHP is demonstrated under any circumstances, attending to environmental parameters.

Table 5
Main assumptions for the TEWI analysis.

Parameter	Value	Direct (D) or Indirect (I)
GWP	2 CO_2e	D
Refrigerant charge	11 kg	D
Annual refrigerant leakages	10%	D
Lifetime	15 years	Both
% recovered at the lifetime	85%	D
Operating hours	8000 h	I
Power consumption	Function of experimental COP	I
Electricity carbon emission factor (2021 values)	Sweden: 12 gCO_2e, Brazil: 142 gCO_2e, USA: 357 gCO_2e, China: 541 gCO_2e	I

3.4. Case studies using experimental results

Although a promising energy recovery opportunity, low-temperature waste heat has challenges associated with its recovery. Finding practical applications for recovered low-temperature waste heat is essential for deploying industrial heat pumps [51]. This section briefly exposes two industrial applications based on the R-1336mzz(Z) experimental measurements presented in this paper. These results can be used as an indicator of the HTHP suitability under different conditions and as a justification for further detailed work, theoretical or experimental.

The points of interest were selected assuming typical operational conditions in different industries: heat source outlet temperatures of 70 and 80 °C and heat sink outlet (production) temperatures of 130 and 157.5 °C (equivalent to steam production at 150 °C) is established. The semi-empirical model was used through linear interpolation of the experimental measurements and calculations and, considering the same LSHX thermal effectiveness and compressor efficiencies.

The main conditions and results of the proposed cases (S1 to S4) are summarised in Table 6. Increasing the heat source outlet temperature by 10 °C (and evaporation temperature) causes a 33% higher heating capacity production and a 17% to 22% COP increment. Then, increasing the heat sink outlet temperature from 130 to 157.5 °C causes a 33% higher heating capacity and a 17% to 22% COP increment. Then, it reduces the heating capacity by 22% and the COP by approximately 40%. Optimising the heat exchangers connected to the HTHP and adjusting the needs of the process can produce a significant variation in energy consumption and hence, electricity running costs and carbon emissions.

The experimental measurements have been used to develop a semi-empirical model and extrapolate the results to other operational conditions [52]. This way, experimental correlations have been developed based on the experimental data to calculate compressor efficiencies, pressure drops, and other operational parameters influencing HTHP performance. Then, design parameters corresponding to a vapor compression basic cycle with an LSHX configuration were taken. These design parameters are the approach point and pressure drops that affect the evaporator, condenser, and pipelines, efficiency and design pressure drop of the LSHX and compressor efficiency. In this way, the expected results are extracted in an ad-hoc installation in two cases:

Case E1: Production of saturated steam at 4.76 bar (150 °C).
Case E2: Heating a thermal oil flow from 110 to 130 °C.

In both cases, a heating capacity of 4 MW has been proposed, corresponding to approximately 6.5 ton h^{-1} of saturated steam production at 150 °C. Table 7 shows the extrapolated results regarding the power consumed by the compressor, the COP and the volumetric suction flow rate required in the compression system (V_G).

As can be seen, the expected COP to generate steam under the desired conditions with a heat source outlet temperature of 70 °C is 2.43. However, if this condition is considered at 80 °C, the expected COP goes up to 3, representing a COP increase of 23%. Similarly, to achieve a production temperature of 130 °C in a heat transfer fluid, the COP varies between 3.60 and 4.46 depending on the exhaust temperature (COP increase of 23%), 70 °C and 80 °C, respectively. In any extrapolated situation, the COP values can be considered high enough to make the HTHP competitive with natural gas boilers, mainly if based on renewable electricity. Finally, the installation's cost analysis is based on the

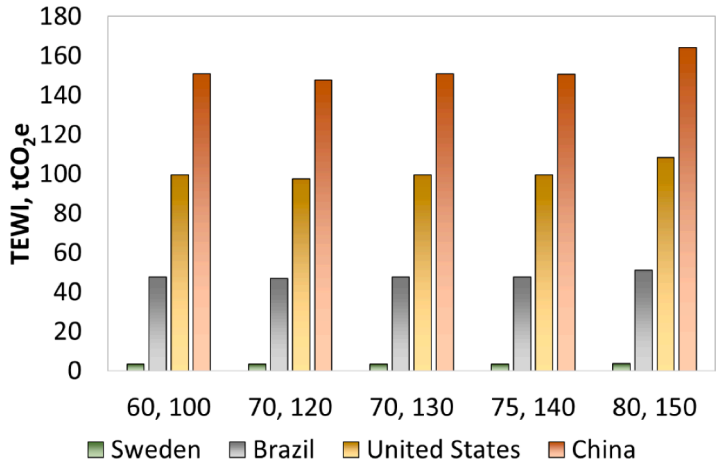

Fig. 13. TEWI results for different evaporation and condensation temperatures and countries.

Table 6
Assumptions and results of industrial case studies.

Condition	$T_{source,in}$	$T_{source,out}$	T_{evap}	$T_{sink,out}$	T_{cond}	PR	T_{disc}	P_{disc}	$\dot{Q}_{cond}$	$\dot{W}_{comp}$	COP
Units	°C	°C	°C	°C	°C	-	°C	bar(a)	kW	kW	–
Case S1	100	70	69.5	130.0	127.4	4.47	139.0	13.13	9.24	3.05	3.03
Case S2	100	80	79.5	130.0	127.4	3.50	139.9	13.47	12.20	3.31	3.69
Case S3	100	70	69.5	157.5	151.8	7.39	166.9	20.79	7.20	3.85	1.87
Case S4	100	80	79.5	157.5	151.8	5.67	167.3	21.12	9.55	4.37	2.19

Table 7
Main results of the HTHP extrapolated cases.

Cases	$T_{source,in}$	$T_{source,out}$	$T_{sink,out}$	$\dot{Q}_{heating}$	$\dot{Q}_{LSHX}$	$\dot{W}_{comp}$	COP	V_G
Units	°C	°C	°C	kW	kW	kW	–	$m^3\ h^{-1}$
Case E1	100	70	150 (saturated vapour)	4000	1781	1643	2.43	8460
		80			1644	1325	3.00	6045
Case E2	100	70	130	4000	1194	1110	3.60	7215
		80			1017	897	4.46	5350

compressor's geometry and operation. Increasing the evaporation temperature by 10 °C would reduce 30% of the compressor required (a combination of displacement and rotational speed). Therefore, HTHP energy efficiency, operational cost and investment are benefitted from a 10 °C higher temperature heat source.

Note that this analysis can be considered conservative because electric and compressor efficiencies are supposed to increase for higher heating capacities. Different compressor technology should be considered in the range of hundreds of kW to MW. These modifications would have implications in the adaptation to pressure range and variable waste heat recovered and heating production. Moreover, the LSHX thermal effectiveness was limited in this lab-scale prototype. However, the LSHX effectiveness could be augmented in future optimized designs for a higher heating capacity and COP. The authors believe that further techno-economic analysis for higher capacities would result in better financial and energy indicators.

4. Conclusions

Additional experiments with organic refrigerants with high critical temperatures are required in the HTHP market. This paper analyses the operational and energy results of R-13336mzz(Z) in an HTHP equipped with a scroll compressor, plate heat exchangers, an electronic expansion valve and an LSHX heat exchanger. The main production temperature reached is approx. 158 °C. The main results are as follows.

A frequency inverter was used to reduce the compressor's frequency from 50 to 40 Hz at higher evaporation temperatures due to limitations in the heating load of the heat source. The evaporation temperature should be increased at higher condensation temperatures to keep the discharge temperature below the limit. Therefore, low-pressure ratios have been tested, between 2.8 and 4.9. For higher condensation temperatures, the pressure ratio was kept nearly constant. Total superheating and subcooling degrees increased because of the higher LSHX thermal effectiveness, which varied between 13% and 39%.

Mass flow rate and heating effect have a contrary contribution on the heating capacity, which resulted from 9.2 to 12.3 kW. Considering the measured power consumption, the heating COP resulted between 4.4 and 1.9. COP values are considered high enough to make this technology attractive in economic and energy terms. SHC COP has also been considered, reaching values from 3.7 to 8.6. This fact evidences the potential of SHC application in industries or district heating and cooling networks to increase the economic viability of HTHPs. Finally, a carbon footprint analysis has proven the convenience of HTHPs even in high carbon emission factor scenarios.

This paper presented the R-1336mzz(Z) operation in an HTHP with LSHX configuration and scroll compressor. However, experimental results are still required with other configurations, refrigerants, and components to determine the combination with the highest energy performance or a trade-off of parameters. These results could also be used for simulating the financial viability of HTHP in different industrial processes and district heating networks, for replacing traditional technologies such as fossil fuel boilers or comparing it with other green

alternatives such as hydrogen or biomass boilers.

Future works focused on techno-economic analysis should consider different heat sink and heat source temperature levels that can be present in the industrial sector assessed. The combination of both parameters significantly influences many HTHP operational and energy parameters, as has been proved in this paper. It is believed that future high-temperature heat pumps will be designed for remarkably higher heating capacity and, therefore, different compressor technology. This can vary compressor efficiency and response to different conditions, such as pressure ratio or adaptation to variable heating capacity. In the financial analysis, researchers are entitled to consider the variation in the cost of electricity required for powering HTHP and fossil fuel used in boilers, as well as the possibility of using thermal storage and renewable sources for electricity production or increasing heat sink temperature.

Declaration of Competing Interest

The authors declare that they have no known competing financial interests or personal relationships that could have appeared to influence the work reported in this paper.

Data availability

Data will be made available on request.

Acknowledgements

Adrián Mota-Babiloni acknowledges grant IJC2019-038997-I funded by MCIN/AEI/10.13039/501100011033. The authors acknowledge project UJI-B2018-24, funded by Universitat Jaume I.

References

[1] United Nations, Adoption of the Paris Agreement, in: Conference of the Parties on Its Twenty-First Session, 2015.
[2] European Commission, Communication from the Commission to the European Parliament, the European Council, the Council, the European Economic and Social Committee and the Committee of the Regions, Eur. Green Deal (2019) 1–24.
[3] European Commission. REPowerEU: affordable, secure and sustainable energy for Europe 2022. https://ec.europa.eu/info/strategy/priorities-2019-2024/european-green-deal/repowereu-affordable-secure-and-sustainable-energy-europe_en (accessed October 11, 2022).
[4] Y. Wang, J. Wang, W. He, Development of efficient, flexible and affordable heat pumps for supporting heat and power decarbonisation in the UK and beyond: review and perspectives, Renew. Sustain. Energy Rev. 154 (2022), 111747, https://doi.org/10.1016/j.rser.2021.111747.
[5] Nowak T. European heat pump market. REHVA federation of european heating, ventilation and air conditioning associations 2022. https://www.rehva.eu/rehva-journal/chapter/european-heat-pump-market (accessed October 11, 2022).
[6] D. Borge-Diez, D. Icaza, D.F. Trujillo-Cueva, E. Açıkkalp, Renewable energy driven heat pumps decarbonization potential in existing residential buildings: roadmap and case study of Spain, Energy 247 (2022), 123481, https://doi.org/10.1016/j.energy.2022.123481.
[7] M.H. Abbasi, B. Abdullah, M.W. Ahmad, A. Rostami, J. Cullen, Heat transition in the European building sector: overview of the heat decarbonisation practices through heat pump technology, Sustain. Energy Technol. Assess. 48 (2021), 101630, https://doi.org/10.1016/j.seta.2021.101630.
[8] G.P. Thiel, A.K. Stark, To decarbonize industry, we must decarbonize heat, Joule 5 (2021) 531–550, https://doi.org/10.1016/j.joule.2020.12.007.
[9] J. Cox, S. Belding, T. Lowder, Application of a novel heat pump model for estimating economic viability and barriers of heat pumps in dairy applications in the United States, Appl. Energy 310 (2022), 118499, https://doi.org/10.1016/j.apenergy.2021.118499.
[10] R. Nandhini, B. Sivaprakash, N. Rajamohan, Waste heat recovery at low temperature from heat pumps, power cycles and integrated systems – Review on system performance and environmental perspectives, Sustain. Energy Technol. Assess. 52 (2022), 102214, https://doi.org/10.1016/J.SETA.2022.102214.
[11] F. Hengel, C. Heschl, F. Inschlag, P. Klanatsky, System efficiency of pvt collector-driven heat pumps, Int. J. Thermofluids 5-6 (2020), 100034, https://doi.org/10.1016/j.ijft.2020.100034.
[12] J. Jiang, B. Hu, R.Z. Wang, N. Deng, F. Cao, C.C. Wang, A review and perspective on industry high-temperature heat pumps, Renew. Sustain. Energy Rev. 161 (2022), 112106, https://doi.org/10.1016/J.RSER.2022.112106.
[13] Arpagaus C., Bless F., Uhlmann M., Schiffmann J., Bertsch S.S. High temperature heat pumps: market overview, state of the art, research status, refrigerants, and application potentials. vol. 152. 2018.
[14] Y. Jovet, F. Lefèvre, A. Laurent, M. Clausse, Combined energetic, economic and climate change assessment of heat pumps for industrial waste heat recovery, Appl. Energy 313 (2022), 118854, https://doi.org/10.1016/J.APENERGY.2022.118854.
[15] T. Rajabloo, W. de Ceuninck, L. van Wortswinkel, M. Rezakazemi, T. Aminabhavi, Environmental management of industrial decarbonization with focus on chemical sectors: a review, J. Environ. Manage. 302 (2022), 114055, https://doi.org/10.1016/j.jenvman.2021.114055.
[16] J. Barco-Burgos, J.C. Bruno, U. Eicker, A.L. Saldaña-Robles, Alcántar-Camarena V. Review on the integration of high-temperature heat pumps in district heating and cooling networks, Energy 239 (2022), 122378, https://doi.org/10.1016/j.energy.2021.122378.
[17] J. Atuonwu, S. Tassou, Decarbonisation of food manufacturing by the electrification of heat: a review of developments, technology options and future directions, Trends Food Sci. Technol. 107 (2021) 168–182, https://doi.org/10.1016/j.tifs.2020.10.011.
[18] M.D. Obrist, R. Kannan, T.J. Schmidt, T. Kober, Long-term energy efficiency and decarbonization trajectories for the Swiss pulp and paper industry, Sustain. Energy Technol. Assessm. 52 (2022), 101937, https://doi.org/10.1016/j.seta.2021.101937.
[19] D. Brough, H. Jouhara, The aluminium industry: a review on state-of-the-art technologies, environmental impacts and possibilities for waste heat recovery, Int. J. Thermofluids 1–2 (2020), 100007, https://doi.org/10.1016/j.ijft.2019.100007.
[20] J.J. Fierro, A. Escudero-Atehortua, C. Nieto-Londoño, M. Giraldo, H. Jouhara, L. C Wrobel, Evaluation of waste heat recovery technologies for the cement industry, Int. J. Thermofluids 7-8 (2020), 100040, https://doi.org/10.1016/j.ijft.2020.100040.
[21] H. Jouhara, A. Żabnieńska-Góra, N. Khordehgah, D. Ahmad, T. Lipinski, Latent thermal energy storage technologies and applications: a review, Int. J. Thermofluids 5-6 (2020), 100039, https://doi.org/10.1016/j.ijft.2020.100039.
[22] J. Jiang, B. Hu, R.Z. Wang, N. Deng, F. Cao, C.-.C. Wang, A review and perspective on industry high-temperature heat pumps, Renew. Sustain. Energy Rev. 161 (2022), 112106, https://doi.org/10.1016/j.rser.2022.112106.
[23] D. Wu, B. Hu, R.Z. Wang, H. Fan, R. Wang, The performance comparison of high temperature heat pump among R718 and other refrigerants, Renew. Energy 154 (2020) 715–722, https://doi.org/10.1016/j.renene.2020.03.034.
[24] O. Bamigbetan, T.M. Eikevik, P. Nekså, M. Bantle, C. Schlemminger, Experimental investigation of a prototype R-600 compressor for high temperature heat pump, Energy 169 (2019) 730–738, https://doi.org/10.1016/J.ENERGY.2018.12.020.
[25] O. Bamigbetan, T.M. Eikevik, P. Nekså, M. Bantle, C. Schlemminger, The development of a hydrocarbon high temperature heat pump for waste heat recovery, Energy 173 (2019) 1141–1153, https://doi.org/10.1016/J.ENERGY.2019.02.159.
[26] M. Verdnik, R. Rieberer, Influence of operating parameters on the COP of an R600 high-temperature heat pump, Int. J. Refrig. (2022), https://doi.org/10.1016/J.IJREFRIG.2022.05.010.
[27] C. Mateu-Royo, J. Navarro-Esbrí, A. Mota-Babiloni, F. Molés, M. Amat-Albuixech, Experimental exergy and energy analysis of a novel high-temperature heat pump with scroll compressor for waste heat recovery, Appl. Energy 253 (2019), https://doi.org/10.1016/j.apenergy.2019.113504. Article 113504.
[28] N. Deng, X. Jing, R. Cai, J. Gao, C. Shen, Y. Zhang, et al., Molecular simulation and experimental investigation for thermodynamic properties of new refrigerant NBY-1 for high temperature heat pump, Energy Convers. Manag. 179 (2019) 339–348, https://doi.org/10.1016/J.ENCONMAN.2018.10.076.
[29] C. Xu, H. Yang, X. Yu, H. Ma, M. Chen, M. Yang, Performance analysis for binary mixtures based on R245fa using in high temperature heat pumps, Energy Convers. Manage.: X 12 (2021), 100123, https://doi.org/10.1016/j.ecmx.2021.100123.
[30] ASHRAE. ANSI/ASHRAE Standard 34–2019 designation and safety classification of refrigerants 2019.
[31] R. Fan, H. Xi, Exergoeconomic optimization and working fluid comparison of low-temperature Carnot battery systems for energy storage, J Energy Storage 51 (2022), 104453, https://doi.org/10.1016/J.EST.2022.104453.
[32] X. Wang, Y. Yan, B. Li, X. Hao, N. Gao, G. Chen, Prospect of solar-driven ejector-compression hybrid refrigeration system with low GWP refrigerants in summer of Guangzhou and Beijing, Int. J. Refrig. 117 (2020) 230–236, https://doi.org/10.1016/J.IJREFRIG.2020.04.035.
[33] S. Malavika, C. Chiranjeevi, Y. Raja Sekhar, T. Srinivas, M. Natarajan, W. Pa Pa Myo, et al., Performance optimization of a heat pump for high temperature application, Mater. Today Proc. 46 (2021) 5278–5285, https://doi.org/10.1016/J.MATPR.2020.08.639.
[34] S. Xiao, D. Nefodov, M.O. McLinden, M. Richter, T. Urbaneck, Working fluid selection for heat pumps in solar district heating systems, Sol. Energy 236 (2022) 499–511, https://doi.org/10.1016/J.SOLENER.2022.02.036.
[35] C. Mateu-Royo, C. Arpagaus, A. Mota-Babiloni, J. Navarro-Esbrí, S.S. Bertsch, Advanced high temperature heat pump configurations using low GWP refrigerants for industrial waste heat recovery: a comprehensive study, Energy Convers. Manag. 229 (2021), 113752, https://doi.org/10.1016/j.enconman.2020.113752.
[36] C. Mateu-Royo, J. Navarro-Esbrí, A. Mota-Babiloni, Á. Barragán-Cervera, Theoretical performance evaluation of ejector and economizer with parallel compression configurations in high temperature heat pumps, Int. J. Refrig. (2020), https://doi.org/10.1016/j.ijrefrig.2020.07.016.
[37] C. Mateu-Royo, J. Navarro-Esbrí, A. Mota-Babiloni, M. Amat-Albuixech, F. Molés, Theoretical evaluation of different high-temperature heat pump configurations for

low-grade waste heat recovery, Int. J. Refrig. 90 (2018) 229–237, https://doi.org/10.1016/j.ijrefrig.2018.04.017.
[38] A. Mota-Babiloni, C. Mateu-Royo, J. Navarro-Esbrí, F. Molés, M. Amat-Albuixech, Á. Barragán-Cervera, Optimisation of high-temperature heat pump cascades with internal heat exchangers using refrigerants with low global warming potential, Energy 165 (2018) 1248–1258, https://doi.org/10.1016/j.energy.2018.09.188.
[39] S. Li, S. He, W. Song, Z. Feng, Thermodynamic analysis of the heat pump steam system with medium-low temperature heat source, Energy Rep. 7 (2021) 266–278, https://doi.org/10.1016/j.egyr.2021.10.032.
[40] A. Fernández-Moreno, A. Mota-Babiloni, P. Giménez-Prades, J. Navarro-Esbrí, Optimal refrigerant mixture in single-stage high-temperature heat pumps based on a multiparameter evaluation, Sustain. Energy Technol.d Assess. 52 (2022), 101989, https://doi.org/10.1016/j.seta.2022.101989.
[41] J. Navarro-Esbrí, A. Fernández-Moreno, A. Mota-Babiloni, Modelling and evaluation of a high-temperature heat pump two-stage cascade with refrigerant mixtures as a fossil fuel boiler alternative for industry decarbonization, Energy 254 (2022), 124308, https://doi.org/10.1016/j.energy.2022.124308.
[42] J. Navarro-Esbrí, F. Molés, B. Peris, A. Mota-Babiloni, K. Kontomaris, Experimental study of an Organic Rankine Cycle with HFO-1336mzz-Z as a low global warming potential working fluid for micro-scale low temperature applications, Energy 133 (2017), https://doi.org/10.1016/j.energy.2017.05.092.
[43] F. Dawo, J. Fleischmann, F. Kaufmann, C. Schifflechner, S. Eyerer, C. Wieland, et al., R1224yd(Z), R1233zd(E) and R1336mzz(Z) as replacements for R245fa: experimental performance, interaction with lubricants and environmental impact, Appl. Energy 288 (2021), 116661, https://doi.org/10.1016/j.apenergy.2021.116661.
[44] C. Arpagaus, S. Bertsch, in: Experimental Comparison of HCFO and HFO R1224yd (Z), R1233zd(E), R1336mzz(Z), and HFC R245fa in a High Temperature Heat Pump up to 150°C Supply Temperature. 18th International Refrigeration and Air Conditioning Conference, Purdue, 2021.
[45] H. Li, P. Hrnjak, Heat transfer coefficient, pressure gradient, and flow patterns of R1233zd(E) and R1336mzz(Z) evaporating in a microchannel tube, Int J Heat Mass Transf 182 (2022), 121992, https://doi.org/10.1016/j.ijheatmasstransfer.2021.121992.
[46] C. Mateu-Royo, J. Navarro-Esbrí, A. Mota-Babiloni, M. Amat-Albuixech, F. Molés, Thermodynamic analysis of low GWP alternatives to HFC-245fa in high-temperature heat pumps: hCFO-1224yd(Z), HCFO-1233zd(E) and HFO-1336mzz (Z), Appl. Therm. Eng. 152 (2019) 762–777, https://doi.org/10.1016/j.applthermaleng.2019.02.047.
[47] E. Huo, C. Liu, X. Xu, Q. Li, C. Dang, S. Wang, et al., The oxidation decomposition mechanisms of HFO-1336mzz(Z) as an environmentally friendly refrigerant in O2/H2O environment, Energy 185 (2019) 1154–1162, https://doi.org/10.1016/j.energy.2019.07.140.
[48] E. Huo, Q. Li, C. Liu, Z. Huang, L. Xin, Experimental and theoretical studies on the thermal stability and decomposition mechanism of HFO-1336mzz(Z) with POE lubricant, J. Anal. Appl. Pyrolysis 147 (2020), 104795, https://doi.org/10.1016/j.jaap.2020.104795.
[49] P. Giménez-Prades, J. Navarro-Esbrí, C. Arpagaus, A. Fernández-Moreno, A. Mota-Babiloni, Novel molecules as working fluids for refrigeration, heat pump and organic Rankine cycle systems, Renew. Sustain. Energy Rev. 167 (2022), 112549, https://doi.org/10.1016/j.rser.2022.112549.
[50] Lemmon E.W., Bell I.H., Huber M.I., McLinden M.O. NIST standard reference database 23: reference fluid thermodynamic and transport properties – REFPROP, version 10.0. NIST 2018.
[51] S. Griffiths, B.K. Sovacool, J. Kim, M. Bazilian, J.M. Uratani, Decarbonizing the oil refining industry: a systematic review of sociotechnical systems, technological innovations, and policy options, Energy Res Soc Sci 89 (2022), 102542, https://doi.org/10.1016/j.erss.2022.102542.
[52] J. Navarro-Esbrí, A. Fernández-Moreno, A. Mota-Babiloni, Modelling and evaluation of a high-temperature heat pump two-stage cascade with refrigerant mixtures as a fossil fuel boiler alternative for industry decarbonization, Energy (2022), 124308, https://doi.org/10.1016/J.ENERGY.2022.124308.